Journal of Sound and Vibration 392 (2017) 187–199

Contents lists available at ScienceDirect

Journal of Sound and Vibration

journal homepage: www.elsevier.com/locate/jsvi

Statistical analysis of vibration in tyres

Alain Le Bot [a,b,*], Zakia Bazari [a,b,c], Philippe Klein [a,c], Joël Lelong [a,c]

[a] Université de Lyon, F-69000 Lyon, France
[b] LTDS-UMR 5513 CNRS-Ecole Centrale de Lyon 36, Avenue Guy de Collongue 69134 Ecully, France
[c] IFSTTAR, AME, LAE, F-69500 Bron, France

ARTICLE INFO

Article history:
Received 10 October 2016
Received in revised form
2 December 2016
Accepted 19 December 2016
Handling Editor: A.V. Metrikine
Available online 29 December 2016

Keywords:
Tyre-road contact
Rolling noise
Modal density
Group speed
Diffuse field

ABSTRACT

The vibration in tyres submitted to random forces in the contact zone is investigated with the model of prestressed orthotropic plate on visco-elastic foundation. It is shown that beyond a cut-on frequency a single wave propagates whose speed is directional-dependent. A systematic numerical exploration of the governing equation solutions shows that three regimes may exist in such plates. These are modal field, diffuse field and free field. For actual tyres which present a high level of damping, the passage from low to high frequencies generally explores the modal and free field regimes but not the diffuse field regime.

1. Introduction

It is commonly acknowledged that traffic generates considerable noise nuisance making our cities as stressful and unpleasant places: the scientific evidence on health effects of environmental noise (in particular of traffic noise) is now well established [1]. Tyre/road interaction noise is the main source of traffic noise for velocities above 40 km/h in normal driving conditions [2]. Furthermore, these last years, substantial progress was performed on the reduction of the engine noise of vehicles, making the rolling noise more perceptible [3].

Several physical mechanisms are responsible for the tyre/road noise generation affecting particular frequency domains, with more or less pronounced contributions depending on the road and tyre characteristics [4]. The main generation mechanisms consist of the tyre belt radiation and air related mechanisms within the contact zone (air-pumping), both influenced by the horn effect. The noise emitted by the tyre structural vibration, reckoned to predominate in the low and medium frequency range, is produced by contact force fluctuations due to the road surface roughness and the tyre tread blocks.

Numerous physical models have been developed to address the tyre belt radiated noise generation, related to either the tyre dynamic behaviour, tyre/road contact or noise radiation from the radial tyre belt velocity. Quite a few provide a complete implementation from road texture data to noise levels (see for instance [5–9]). The vibrational behaviour of the tyre is a key input for these evaluations.

In the literature, two types of vibrating tyre model have been used: numerical and analytical models. In the first category, we usually find finite element models with more or less refinement [10–13]. The advantages of numerical models are their

* Corresponding author at: Université de Lyon, F-69000 Lyon, France.
E-mail address: alain.le-bot@ec-lyon.fr (A. Le Bot).

http://dx.doi.org/10.1016/j.jsv.2016.12.030
0022-460X/

precision in the description of details and their realism. But they are generally time consuming and for this reason limited to low and mid frequencies, although computational costs can be substantially reduced by the waveguide finite element approach [14–17]. In the second category, several authors proposed two-dimensional models [18–20] where the tyre is a circular ring. The advantage of the ring model is its simplicity as well as a good description of the vibration at low frequencies. Soedel and Prasal [21] explored the effect of contact in natural frequencies while more elaborated models have been proposed for higher frequencies [22]. In Ref. [9], Kropp proposed a simple analytical model where the tyre including the belt and sidewalls is approached by a prestressed orthotropic thin plane plate on an elastic foundation. This model valid above the ring frequency has the advantage that the modal basis is known analytically which drastically simplifies the computations [23].

This paper outlines the question of the characterisation of vibrations in tyres with the model of prestressed orthotropic plate on a visco-elastic foundation. In contrast with previous studies of tyre vibration, we shall adopt a double point of view based on statistical considerations and an energetic approach. The statistical point of view means that we shall not try to investigate the details of the vibration field or the properties of a particular mode, but, only their overall features when all modes respond to a broadband random force. We shall obtain a classification in only three types of energy repartition, one type when the response is dominated by few modes, a second type is the diffuse field state and the third one is when rays are highly absorbed with a domination of the direct field.

The paper is organised as follows. In Section 2, we present the model of tyre in contact with a rough road. In Section 3 the main statistical parameters that drive the behaviour of vibrational field in tyres are introduced. Then we present in Section 4 a numerical evidence of the existence of three vibrational regimes in tyres. In Section 5, the effect of the contact area is discussed and the previous observations are adjusted. Some conclusions are given in Section 6.

2. Description of the tyre model

Due to loading, the tyre deforms on the road surface to make a contact zone of a few tens of square centimetres. Contact forces are generated at the tyre/road interface whose fluctuations due to rolling create vibrations of the tyre belt. Out-of-plane vibrations with respect to the steady state tyre deformation are of importance for noise generation. We adopt the analytical model of prestressed orthotropic plate on visco-elastic stiffness as proposed in Ref. [9]. The Green's function is given in Ref. [23]. The tyre is virtually unwrapped in the circumferential and lateral directions as a plate (Fig. 1). It is considered periodic in the circumferential direction and fixed at the rim on both lateral edges. The tension in the plate and the visco-elastic bedding are due to the tyre inflation. The normal displacement of the plate stands for the radial displacement on the real tyre.

2.1. Random force

The tyre is excited by time-varying external forces whose origin is the mechanical contact between tyre and road. During the rolling process, a point in the tyre tread which enters into the contact zone submits a normal force in the radial direction. This force is relaxed when the point leaves the contact zone. Furthermore, the topography of road and texture of the tyre tread induces temporal fluctuations of the force during the passage in the contact zone. Of course, a complete determination of the force field is a complex problem of contact mechanics that requires in general a high quantity of computations [24,25]. However, for the sake of simplicity, we shall only retain in the model the main features of the force field.

The most important characteristic of contact forces is their random nature whose origin stems from the random nature of the road surface. The time-correlation of the force is of order of the passage time of an asperity into the contact zone that is few milliseconds. Whereas the spatial-correlation of contact pressure is of order of the asperity size that is few millimetres. The force pressure may therefore be conveniently modelled as a stochastic process δ-correlated in time and space. For such a “rain-on-the-roof” excitation, the power spectral density S_0 is the same at any point and is constant in frequency. The analysis of vibration will be conducted in frequency bands $\Delta\omega$ centred on ω_0 taken conventionally as octave bands. Since the power spectral density is constant, the root mean square value of force in $\Delta\omega$ is

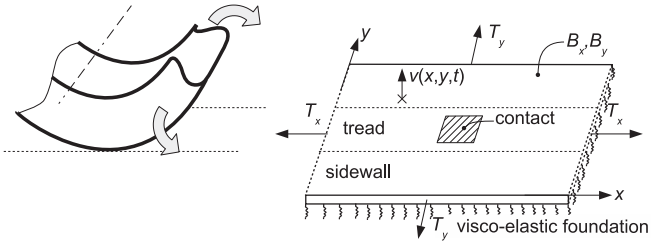

Fig. 1. Tyre-road model. Left, the tyre is virtually unwrapped. Right, equivalent prestressed orthotropic plate under visco-elastic foundation.

$$f_{\mathrm{rms}} = \sqrt{S_0 \Delta\omega} \tag{1}$$

This simplified model of contact forces is well supported by experimental observations [26].

2.2. Prestressed orthotropic plate on visco-elastic foundation

The governing equation for out-of-plane vibrations in a prestressed orthotropic plate on a visco-elastic foundation is

$$\left[\left(\sqrt{B_x}\frac{\partial^2}{\partial x^2} + \sqrt{B_y}\frac{\partial^2}{\partial y^2}\right)^2 - \left(T_x\frac{\partial^2}{\partial x^2} + T_y\frac{\partial^2}{\partial y^2}\right) + S + c\frac{\partial}{\partial t} + m\frac{\partial^2}{\partial t^2}\right] v = f(x, y, t) \tag{2}$$

where $v(x, y, t)$ is the displacement field in direction normal to the plate and $f(x, y, t)$ is the contact force field. In the above equation, m denotes the mass per unit area in kg/m^2, T_x (resp. T_y) is the x-component (resp. y-component) of the tensile force in N/m imposed by the air pressure (always positive), B_x (resp. B_y) is the bending stiffness in the x-direction (resp. the y-direction) in N m, S is the stiffness per unit area in N/m^3 of the elastic foundation, and c a viscous damping coefficient in N s/m^3.

In the circumferential direction, the tyre is assimilated a cylinder of perimeter a. The equivalent plane plate must therefore satisfy four periodic conditions

$$v(0, y, t) = v(a, y, t) \tag{3}$$

$$\frac{\partial v}{\partial x}(0, y, t) = \frac{\partial v}{\partial x}(a, y, t) \tag{4}$$

$$\frac{\partial^2 v}{\partial x^2}(0, y, t) + \nu_y\frac{\partial^2 v}{\partial y^2}(0, y, t) = \frac{\partial^2 v}{\partial x^2}(a, y, t) + \nu_y\frac{\partial^2 v}{\partial y^2}(a, y, t) \tag{5}$$

$$\frac{\partial^3 v}{\partial x^3}(0, y, t) + (2 - \nu_y)\frac{\partial^3 v}{\partial x \partial y^2}(0, y, t) = \frac{\partial^3 v}{\partial x^3}(a, y, t) + (2 - \nu_y)\frac{\partial^3 v}{\partial x \partial y^2}(a, y, t) \tag{6}$$

where ν_x and ν_y are the Poisson coefficients respectively in directions x and y. The four conditions give respectively the continuity of deflection, rotation, moment and shear force.

At the edges of sidewalls, the tyre is fixed on the rim so that the vibration is zero on the edges but a rotation is allowed by deformation of the elastomer. The most simple and idealised conditions for a plate of width b are the simply supported boundary conditions,

$$v(x, 0, t) = 0 \tag{7}$$

$$v(x, b, t) = 0 \tag{8}$$

$$\frac{\partial^2 v}{\partial y^2}(x, 0, t) + \nu_x\frac{\partial^2 v}{\partial x^2}(x, 0, t) = 0 \tag{9}$$

$$\frac{\partial^2 v}{\partial y^2}(x, b, t) + \nu_x\frac{\partial^2 v}{\partial x^2}(x, b, t) = 0 \tag{10}$$

We may remark that in Eqs. (9) and (10) all partial derivatives with respect to x vanishes since the function $x \mapsto v(x, 0, t)$ is null (idem for $x \mapsto v(x, b, t)$). A similar remark applies to Eq. (5). The equality of functions $y \mapsto v(0, y, t)$ and $y \mapsto v(a, y, t)$ implies the equality of their second spatial derivatives with respect to y. For Eq. (6), the equality of the third derivative with respect to x and y comes from Eq. (4). We therefore obtain an equivalent set of boundary conditions by cancelling all terms where ν_x or ν_y appears in Eqs. (3)–(10).

The mode shapes of the above boundary value problem are

$$\psi_{ij1}(x, y) = a_{ij}\cos\left(2i\pi\frac{x}{a}\right)\sin\left(j\pi\frac{y}{b}\right) \quad i = 0, 1, \ldots\ j = 1, 2, \ldots \tag{11}$$

$$\psi_{ij2}(x, y) = b_{ij}\sin\left(2i\pi\frac{x}{a}\right)\sin\left(j\pi\frac{y}{b}\right) \quad i = 1, 2, \ldots\ j = 1, 2, \ldots \tag{12}$$

In the above expression, the subscript i starts at 0 in ψ_{ij1} and 1 in ψ_{ij2} while j always starts at 1. The normalizing factors a_{ij} and b_{ij} are given by

$$\int_0^a \int_0^b \left[\psi_{ijk}(x, y)\right]^2 \mathrm{d}x\mathrm{d}y = 1 \tag{13}$$

We get $a_{ij} = \sqrt{2/(ab)}$ if $i=0$ and $a_{ij} = b_{ij} = 2/\sqrt{ab}$ otherwise. The eigenvalues of these eigenmodes are

$$m\omega_{ij}^2 = \left[\sqrt{B_x}\left(\frac{2i\pi}{a}\right)^2 + \sqrt{B_y}\left(\frac{j\pi}{b}\right)^2\right]^2 + \left[T_x\left(\frac{2i\pi}{a}\right)^2 + T_y\left(\frac{j\pi}{b}\right)^2\right] + S \tag{14}$$

where ω_{ij} is the natural frequency (rad/s) of mode i, j. Note that modes (i, j, k), $k=1,2$ are degenerated when $i \geq 1$ and form an eigenspace of dimension 2.

For the sake of simplicity, we shall write the mode shapes $\psi_\alpha(\mathbf{x})$ where $\alpha = (i, j, k)$ is a triple subscript and $\mathbf{x} = (x, y)$ is a point. The transfer mobility (frequency response function between a force applied at $\mathbf{x}_0$ and the vibrational velocity at $\mathbf{x}$) is then

$$Y(\mathbf{x}, \mathbf{x}_0; \omega) = \mathrm{i}\omega \sum_\alpha \frac{\psi_\alpha(\mathbf{x})\psi_\alpha(\mathbf{x}_0)}{m\left(\omega_\alpha^2 + \mathrm{i}\eta_\alpha\omega\omega_\alpha - \omega^2\right)} \tag{15}$$

where ω_α denotes ω_{ij}, $\eta_\alpha = c/(m\omega_\alpha)$ is the damping loss factor and $\mathrm{i} = \sqrt{-1}$ the complex imaginary unit. After simplifying

$$Y(\mathbf{x}, \mathbf{x}_0; \omega) = \mathrm{i}\omega \sum_{i\geq 0,\, j\geq 1} \frac{4\epsilon_i}{ab} \frac{\cos\left(2i\pi\frac{x-x_0}{a}\right)\sin\left(j\pi\frac{y}{b}\right)\sin\left(j\pi\frac{y_0}{b}\right)}{m\left(\omega_{ij}^2 + \mathrm{i}\eta_{ij}\omega\omega_{ij} - \omega^2\right)} \tag{16}$$

where $\epsilon_0 = 1/2$ and $\epsilon_i = 1$ for $i > 0$.

2.3. Numerical values

Typical values for the orthotropic plate parameters can be found in the literature [9,27,28]. Geometrical parameters and mass per unit area can be measured directly. The determination of other parameters is not straightforward. They are determined from point mobility measurement results. In Ref. [27], parameters are identified by curve fitting between the measured and calculated mobility using a Simplex search method. In Ref. [28], the bedding stiffness, bending stiffness in circumferential and lateral directions and tension are determined separately by physical considerations. The numerical values of physical parameters are those of a radial slick tyre 155/70R13 inflated at 2 bars given in Ref. [27]. They are listed in Table 1 while the first natural frequencies are given in Table 2.

3. Statistical properties of tyres

In this section, we introduce the main parameters relevant to a statistical description of vibrational field on a tyre.

3.1. Wave speed

The wave propagation analysis is conducted in the undamped case ($c=0$). Let us consider a plane wave propagating in direction θ with respect to the circumferential direction. The θ-travelling wave is of the form $v(x, y, t) = \exp(-\mathrm{i}kx\cos\theta - \mathrm{i}ky\sin\theta + \mathrm{i}\omega t)$ where the wavenumber vector is $(k\cos\theta, k\sin\theta)$. The dispersion relationship is obtained by substituting this solution in the undamped governing equation. It gives

$$Bk^4 + Tk^2 + S - m\omega^2 = 0 \tag{17}$$

where B (resp. T) denotes the effective bending stiffness (resp. effective tension) in direction θ. They are given by

$$B(\theta) = \left(\sqrt{B_x}\cos^2\theta + \sqrt{B_y}\sin^2\theta\right)^2 \tag{18}$$

$$T(\theta) = T_x\cos^2\theta + T_y\sin^2\theta \tag{19}$$

Eq. (17) is a biquadratic polynomial equation. Let $X = k^2$, the discriminant of $P(X) = BX^2 + TX + S - m\omega^2$ is

Table 1
Parameter numerical values of the orthotropic plate under tension and on elastic foundation.

Parameter	a	b	m	B_x	B_y	T_x	T_y	S
Units	m	m	kg/m^2	N m	N m	N/m	N/m	N/m^3
Value	1.78	0.32	12.4	20	8	3×10^4	8×10^4	1.3×10^6

Table 2
Natural frequencies of the orthotropic plate under tension and on elastic foundation.

Mode (i,j)	(0, 1)	(1, 1)	(2, 1)	(3, 1)	(4, 1)	(5, 1)	(6, 1)	(0, 2)	(1, 2)	(2, 2)
Frequency (Hz)	134.0	137.0	146.1	160.9	181.0	206.3	236.4	259.8	261.7	267.6

$\Delta = T^2 - 4B(S - m\omega^2)$. It is non-negative when $m\omega^2 \geq S - T^2/4B$. But the numerical values of Section 2.3 indicates that $S - T^2/4B < 0$ and thus $\Delta \geq 0$ for all $\omega \geq 0$. The two roots of $P(X)$ are

$$X_1 = \frac{-T - \sqrt{\Delta}}{2B} \tag{20}$$

$$X_2 = \frac{-T + \sqrt{\Delta}}{2B} \tag{21}$$

The first root is always negative. The related wavenumbers $k = \pm\sqrt{X_1}$ are purely imaginary and therefore give rise to evanescent waves. The second root X_2 may be positive or negative. Its sign depends on the cut-on frequency

$$\omega_{\text{cut-on}} = \sqrt{\frac{S}{m}} \tag{22}$$

When $\omega < \omega_{\text{cut-on}}$, $X_2 < 0$ and again the associated waves are evanescent. Thus, no wave propagates in the plate below $\omega_{\text{cut-on}}$. When $\omega \geq \omega_{\text{cut-on}}$, $X_2 \geq 0$ and we obtain two propagating waves whose wavenumbers are $\pm k(\omega)$ with

$$k(\omega) = \sqrt{\frac{-T + \sqrt{T^2 - 4B(S - m\omega^2)}}{2B}} \tag{23}$$

In summary, in a plate whose governing equation is Eq. (2), no wave can propagate below the cut-on frequency given in Eq. (22). Above the cut-on frequency, a single wave can propagate whose wavenumber is given in Eq. (23). The phase speed is

$$c_\varphi = \frac{\omega}{k(\omega)} \tag{24}$$

while the group speed is

$$c_g = \frac{\mathrm{d}\omega}{\mathrm{d}k} = \frac{1}{k'(\omega)} \tag{25}$$

where $k'(\omega)$ is the derivative of k with respect to ω.

Fig. 2 shows the four wavenumbers solution to Eq. (17) in the complex plane for all $\omega \geq 0$. The four wavenumbers are purely imaginary at $\omega = 0$ (circles in Fig. 2) and do not lead to propagation of waves. Two wavenumbers remain purely imaginary and goes to $\pm i\infty$ when $\omega \to \infty$. The two others are first purely imaginary and then purely real above the cut-on frequency (see the inset). They go to $\pm\infty$ when $\omega \to \infty$. These wavenumbers are responsible of propagation in tyres.

The phase and group velocities of a right-travelling wave are shown in Fig. 3. The cut-on frequency is 45 Hz. No wave can

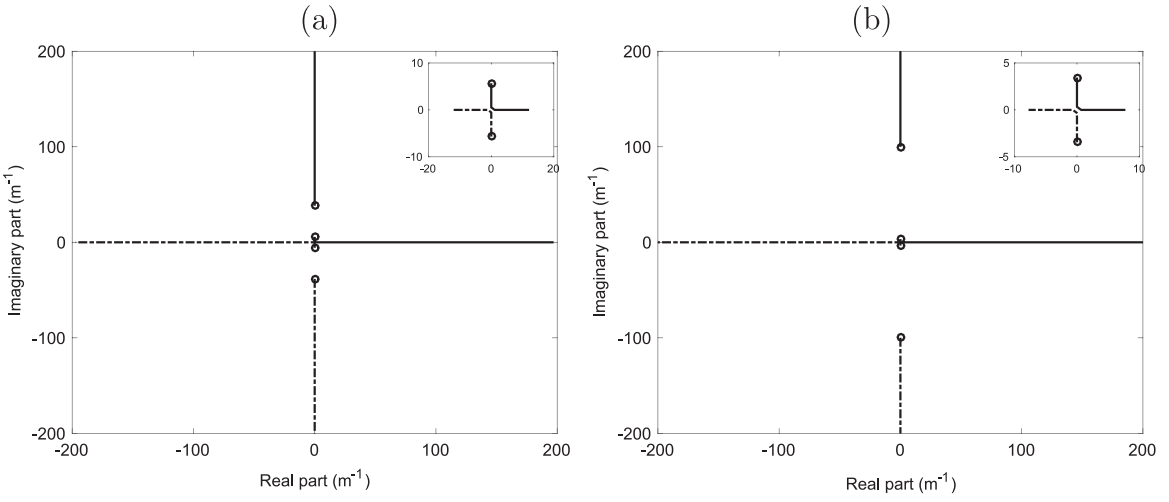

Fig. 2. Wavenumbers in tyres represented in the complex plane versus frequency: (a) circumferential direction; (b) lateral direction. At $\omega = 0$ the four wavenumbers (o) are purely imaginary. The transition to real wavenumbers (inset) takes place at the cut-on frequency.

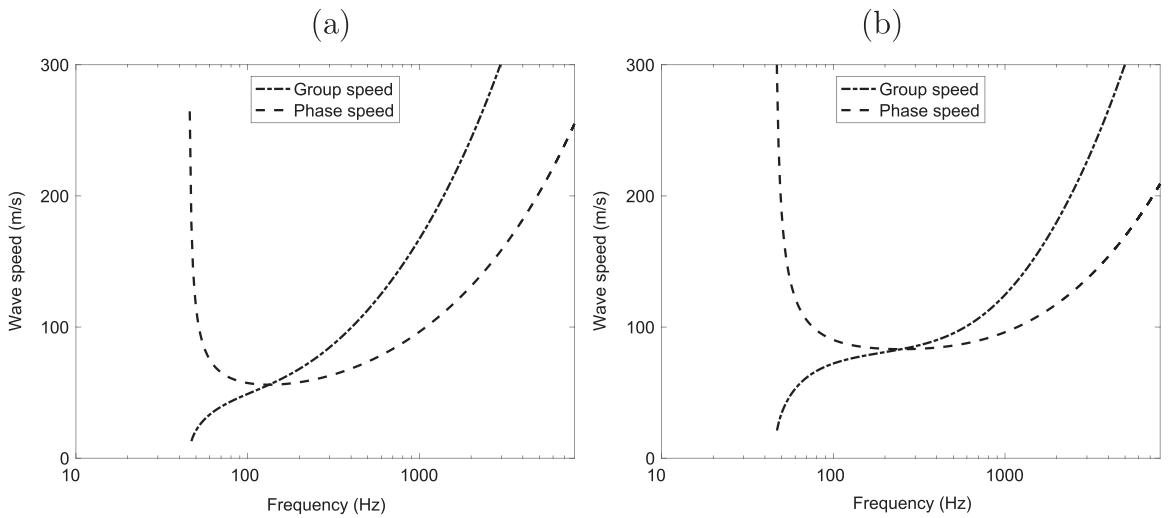

Fig. 3. Wave speeds in tyres: (a) circumferential direction; (b) lateral direction. The cut-on frequency is 45 Hz.

propagate below the cut-on frequency while only one wave propagates above the cut-on frequency. The group speed is an increasing function of frequency. The group speed is very low just above the cut-on frequency and has a point of inflection about 100 Hz (circumferential) or 200 Hz (lateral). Above inflection, the group speed increases more rapidly. The phase speed is first a strongly decreasing function of frequency just above the cut-on frequency. It is stable in the range 100–400 Hz (circumferential) or 100–800 Hz (lateral) with a minimum value of 56 m/s (circumferential) and 83 m/s (lateral). Above this transition range, the phase speed increases like $\omega^{1/2}$.

In the asymptotic limit $\omega \to \infty$, it may be seen from Eq. (23) that the phase velocity is $(B/m)^{1/4}\omega^{1/2}$ and the group speed is $c_g = 2c_\varphi$ which are the velocities in a simple plate in transverse vibration (no prestress and no elastic foundation). The domain of high frequencies is therefore dominated by the bending effect. But at low frequencies between the cut-on frequency and 400 Hz, we observe a large difference between phase and group speeds which cannot be reduced to a constant ratio. This domain is dominated by the effect of the elastic foundation which imposes a cut-on in wave propagation and therefore an arbitrarily high phase speed. These observations are in agreement with previous studies [19].

3.2. Number of modes

The first statistical parameter of interest is the number of modes in the frequency band $\Delta\omega$ also called mode count. This parameter is denoted as $N(\omega)$ in the following. A dual parameter is the modal density defined by $n(\omega) = N(\omega)/\Delta\omega$. The modal density is the mean number of modes per unit frequency (in rad/s). The modal density may be assessed by at least three methods.

The most direct method consists in an analytic count by calculating all eigenfrequencies with Eq. (14). The resonant modes are those whose natural frequency is within $\Delta\omega$. Their number $N(\omega)$ and therefore the modal density $n(\omega)$ is determined by a simple algorithm. This may be written

$$n(\omega) = \frac{1}{\Delta\omega}\Big[\mathrm{Card}\left\{j \geq 1 | \omega_{0j} \in \Delta\omega\right\} + 2 \times \mathrm{Card}\left\{i \geq 1, j \geq 1 | \omega_{ij} \in \Delta\omega\right\}\Big] \tag{26}$$

where Card denotes the cardinal number of the set of integers i, j for which the natural frequency ω_{ij} is contained in the frequency band $\Delta\omega$. The two terms correspond to the two cases $i=0$ and $i \geq 1$. In the case $i=0$ a single mode is present while two modes are attached to each couple i, j when $i \geq 1$. This explains the presence of the factor 2 in the second term.

A second method is based on an asymptotic estimation of the modal density. The modal density of a general anisotropic plate has been studied by Langley [29]. If the plate has area $A=ab$ and waves travel at group speed $c_g(\theta)$ and phase speed $c_\varphi(\theta)$ in direction θ, then the modal density is

$$n(\omega) = \frac{A\omega}{2\pi^2}\int_0^\pi \frac{\mathrm{d}\theta}{c_\varphi(\theta)c_g(\theta)} \tag{27}$$

Let us remark that for Love plates ($T_x = T_y = S = 0$ and $B_x=B_y$) c_g and c_φ are proportional to the root mean square of the frequency and therefore the modal density is constant for all frequencies. But in general the proportionality $c_\varphi,\ c_g \propto \omega^{1/2}$ does not hold and the modal density is not constant.

The third approach is an estimation of the modal density by the mean mobility. Bourgine [30] proposed to estimate the modal density by

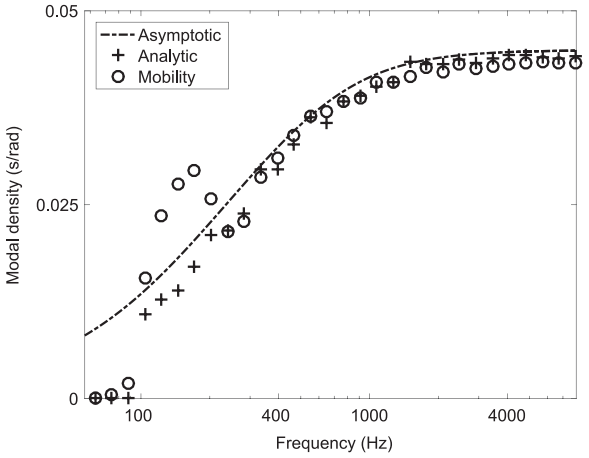

Fig. 4. Modal density in tyres versus frequency. +, analytic count of modes by Eq. (26); −., asymptotic estimation by Eq. (27); o, mean mobility estimation by Eq. (28). In the asymptotic limit $\omega \to \infty$ the modal density is constant.

$$n(\omega) = \frac{2M}{\pi A \Delta\omega} \int_A \int_{\Delta\omega} \mathrm{Re}\left[Y(\mathbf{x}, \mathbf{x}; \omega) \right] \mathrm{d}\omega \mathrm{d}A_{\mathbf{x}} \tag{28}$$

where $Y(\mathbf{x}, \mathbf{x}; \omega)$ is the point mobility at $\mathbf{x}$ and Re denotes the real part. Eq. (28) shows that the spatial and frequency average the driving-point conductance (real part of the mobility) is proportional to the number of modes in the frequency bandwidth. The main interest of Eq. (28) is that it allows a direct measurement of the modal density. For this purpose, the driving-point mobility must be measured over the frequency band of interest in several positions on the tyre and then averaged for all these positions. In practice, few points are necessary to get a good estimation of the modal density.

Fig. 4 shows the modal density estimated by the above three methods. We can observe that in the asymptotic limit $\omega \to \infty$ the modal density reaches a limit. This is consistent with the fact that the plates behaviour is dominated by flexural effects at high frequencies and therefore the modal density becomes constant as for any Love plate. But at low frequencies, the modal density has a more complicated behaviour. Its limit is zero in the neighbourhood of $\omega_{\mathrm{cut-on}}$ since the phase speed becomes infinite. The estimation by the mean mobility is done with a single point (the source position $\mathbf{x}_0$). It may be seen that the estimation is quite good excepted below 300 Hz. This shows that Eq. (28) is robust even with a single point mobility.

The mode count gives the size of the population of resonant modes. Due to their frequency proximity with excitation, the resonant modes are the main contributors to the vibration. The size of the population of modes is the first criterion to check before to adopt a statistical description of the vibrational field. For instance at 1 kHz, the number of resonant modes in an octave is $N = 192$ which is usually enough to treat them as a statistical population by forgetting their exact natural frequencies.

3.3. Modal overlap

The second statistical parameter is the modal overlap. The modal overlap is defined by

$$M(\omega) = \eta(\omega)\omega n(\omega) \tag{29}$$

where $\eta(\omega)$ is the mean damping loss factor at frequency ω (over a significant number of modes about ω) and $n(\omega)$ the modal density.

The modal overlap is a measure of the overlapping of successive modes. If $\Delta = \eta\omega$ denotes the half-power bandwidth (width of a frequency peak at −3 dB) of a mode at frequency ω and $1/n$ the mean frequency span between two successive modes, then the modal overlap is the ratio between the half-power bandwidth and the mean frequency span. A modal overlap of 1 means that a resonance peak can emerge by only 3 dB before the following mode starts to emerge.

The modal overlap allows to distinguish two regimes in tyres. When the modal overlap is low (see Fig. 5a), the resonance peaks are well separated in the mobility function. All resonances are clearly visible on the mobility and for instance the experimental modal analysis will be efficient to identify the modes. In this modal regime, all modes take part of overall dynamics and the exact knowledge of their natural frequencies and shapes is of a great importance to characterise the vibrational field. But when the modal overlap is high (see Fig. 5b) most of modes overlap and their frequency peaks are usually no longer visible on the mobility. In the extreme case of a very large modal overlap, peaks can totally vanish and the frequency response function is smooth. Modes always exist but they cannot be identified by a modal analysis. The precise values of their natural frequencies have a weak influence on the mobility and more generally on the vibrational field. In this regime of high modal overlap, modes are not distinguishable and loss their individuality. Their utility in an effective computation of the vibrational field is therefore questionable. In this regime, a statistical analysis is of course well suited for a description of the vibrational field.

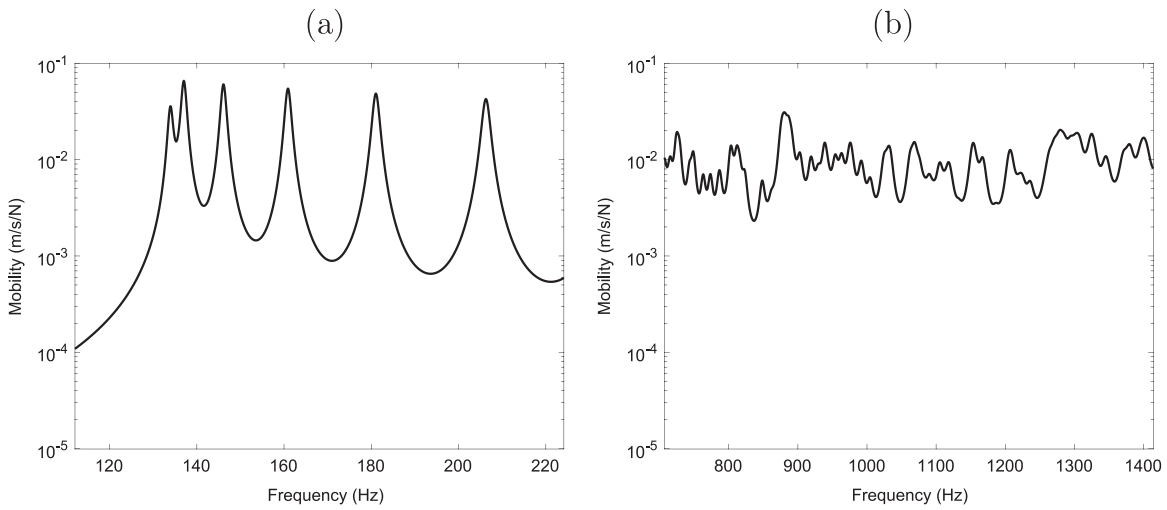

Fig. 5. Effect of modal overlap on mobility. (a), low modal overlap $M=0.2$ and low mode count $N=6$. The peaks of eigenfrequencies are well separated. (b), high modal overlap $M=3$ and high mode count $N=192$. Most of modes overlap and are not distinguishable.

3.4. Attenuation of waves

The third statistical parameter is related to wave attenuation. During their travel in tyres, vibrational rays continuously loss energy by dissipation processes in material and ultimately vanish after a certain distance. The attenuation of waves therefore tends to confine the energy in the vicinity of the source point. But before to vanish, the rays hit the boundaries and are reflected several times. The multiple reflections are responsible of a mixing of energy in the plate. Thus, these two processes attenuation and reflection are in competition, the former being responsible of a confinement of energy while the second one tends to mix energy inside the tyre.

The mean free path is the mean length between two successive reflections of a ray. Since the tyre is modelled by a periodic plate simply supported on the lateral edges, reflections can occur only on lateral edges. This problem is geometrically equivalent to that of rays travelling in an infinite band strip of same width. The mean free path in a tyre is therefore

$$l = \frac{\pi b}{2} \tag{30}$$

where b is the tyre width. The inverse of the mean free path $1/l$ is the number of reflections per unit length while c_g/l is the mean number of reflections per unit time. In the tyre specified by the numerical values of parameters given in Section 2.3, the mean free path is 0.5 m which corresponds to 209 reflections per second at 1 kHz.

Dissipation in material imposes a decreasing of energy. The energy of rays follows a time-decreasing exponential law $\exp(-\eta\omega t)$. The loss of energy per unit time is $\exp(-\eta\omega)$. If we admit that the rays disappear when their energy comes down, say below 1% of their initial energy, then the time life of a ray in a tyre at 1 kHz and $\eta = 10\%$ is 7 ms. Since the speed of propagation of energy is the group velocity c_g, the distance-decreasing law of energy is $\exp(-\eta\omega x/c_g)$. With the same criterion of 1%, the distance travelled by a ray at 1 kHz with a typical group speed $c_g=140$ m/s and $\eta = 10\%$ is 1.0 m. This corresponds to only one or two reflections.

The above two parameters, mean free path l and attenuation per unit length $\eta\omega/c_g$, combine into a single dimensionless parameter $\eta\omega l/c_g$. Since the tyre is not isotropic, c_g depends on the direction of propagation just as the dimensionless parameter. For a ray with a unit initial energy and a random direction, its mean energy after a mean free path is

$$\frac{1}{2\pi}\int_0^{2\pi} \exp\left(-\frac{\eta\omega}{c_g}l\right) \mathrm{d}\theta$$

We may introduce the normalised attenuation factor

$$m(\omega) = -\ln\left[\frac{1}{2\pi}\int_0^{2\pi} \exp\left(-\frac{\eta\omega}{c_g}l\right)\mathrm{d}\theta\right] \tag{31}$$

as the ratio of energy lost during a travel of length the mean free path. Note that for isotropic plates, this definition of the normalised attenuation factor reduces to $m = \eta\omega l/c_g$ which is that given in Ref. [31]. The normalised attenuation factor measures the number of reflections undergone by a ray during its time life. A small value of normalised attenuation means a large number of reflections and therefore a state of mixing energy (Fig. 6a). Conversely, a large value of normalised attenuation leads to a confinement of the energy in the vicinity of the source point (Fig. 6b).

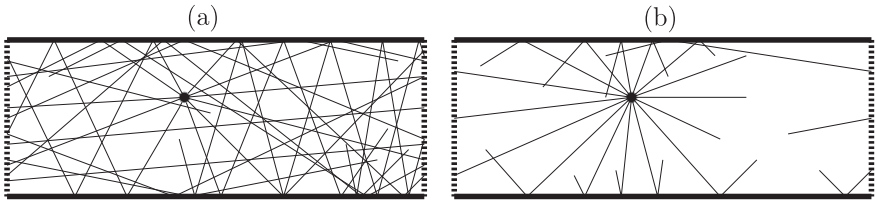

Fig. 6. Effect of wave attenuation on the vibrational field. (a), low attenuation. A long propagation ensures a large number of reflections of rays and therefore a mixing of energy (b), high attenuation. The rays are strongly absorbed and vanish after the first reflections leading to the dominance of the free field.

4. Vibrational regimes in tyres

This section presents the classification of vibrational regimes in tyres by their types of spatial repartition of energy.

4.1. Definition of the local energy

Let us first define the local vibrational energy. The tyre is assimilated to a prestressed orthotropic plate on visco-elastic foundation excited by a random point force. At any point $\mathbf{x}$ of the plate, the twice of kinetic energy density is $m\dot{v}^2(\mathbf{x}, t)$ where the dot denotes a time-derivative and m the mass per unit area. But the force is random, stationary and has a flat spectrum confined in the frequency band $\Delta\omega$ about ω_0. We therefore introduce the random expectation of energy

$$E(\mathbf{x};\, \omega_0) = \langle m\dot{v}^2(\mathbf{x}, t)\rangle \tag{32}$$

where the brackets denote the expectation operator. Of course, the expectation of local energy E still depends on the variable $\mathbf{x}$ but not on time by virtue of stationarity of forces. The variable ω_0 also appears in E to remind the centre frequency of excitation.

In Eq. (32), the product $\langle \dot{v}^2(\mathbf{x}, t)\rangle$ may be interpreted as the auto-correlation function of vibrational speed $R_{\dot{v}\dot{v}}(\tau) = \langle v(\mathbf{x}, t+\tau)v(\mathbf{x}, t)\rangle$ taken at $\tau = 0$. But it is well-known [32] that $R_{\dot{v}\dot{v}}(0) = \int S_{\dot{v}\dot{v}}(\omega)\, \mathrm{d}\omega/2\pi$ where $S_{\dot{v}\dot{v}}(\omega)$ is the power spectral density of $\dot{v}$. Since the system is linear, $S_{\dot{v}\dot{v}}$ is given by $S_{\dot{v}\dot{v}}(\omega) = |Y(\mathbf{x}, \mathbf{x}_0, ;\, \omega)|^2 S_0$ where S_0 is the power spectral density of the force f at $\mathbf{x}_0$ and Y the frequency response function between $\dot{v}$ at $\mathbf{x}$ and f at $\mathbf{x}_0$ (transfer mobility). One obtains the expectation of local vibrational energy as

$$E(\mathbf{x};\, \omega_0) = S_0 \int_{\Delta\omega} m\,|Y(\mathbf{x}, \mathbf{x}_0;\, \omega)|^2 \mathrm{d}\omega \tag{33}$$

The range of integration is $\Delta\omega$ since S_0 and therefore $S_{\dot{v}\dot{v}}$ is zero outside $\Delta\omega$.

4.2. Spatial repartition of energy

We can now examine the spatial repartition of energy. The spatial average of vibrational energy estimated on the whole plate A is

$$\overline{E}(\omega_0) = \frac{1}{A}\int_A E(\mathbf{x};\, \omega_0)\mathrm{d}A_{\mathbf{x}} \tag{34}$$

The spatial repartition of energy is characterised by the mean value and standard deviation. We may therefore introduce the relative standard deviation

$$\sigma = \frac{1}{\overline{E}(\omega_0)}\sqrt{\frac{1}{A}\int_A E(\mathbf{x};\, \omega_0)^2 \mathrm{d}A_{\mathbf{x}} - \overline{E}(\omega_0)^2} \tag{35}$$

as the ratio of spatial standard deviation of local energy and mean energy. The ratio σ characterises the uniformity of spatial repartition. Its definition is quite similar to the relative variance of the mean squared pressure introduced in room acoustics to characterise the state of diffuse field [33]. Its value gives the relative fluctuations (in percentage of the mean value) of energy from a point to another point of the tyre. Small values of σ therefore indicate a uniform repartition of energy in the whole tyre while large values of σ are representative of strong spatial fluctuations.

4.3. Description of three regimes

The numerical simulation presented in this section is based on the set of mechanical parameters given in Section 2.3. The plate has length $a = 1.78$ m and width $b = 0.32$ m. A point-force drives the plate at $\mathbf{x}_0 = (0.867,\, 0.142)$ (origin of the frame at a plate corner) chosen inside the contact zone in a non-symmetric position to ensure that all modes are excited. The mobility

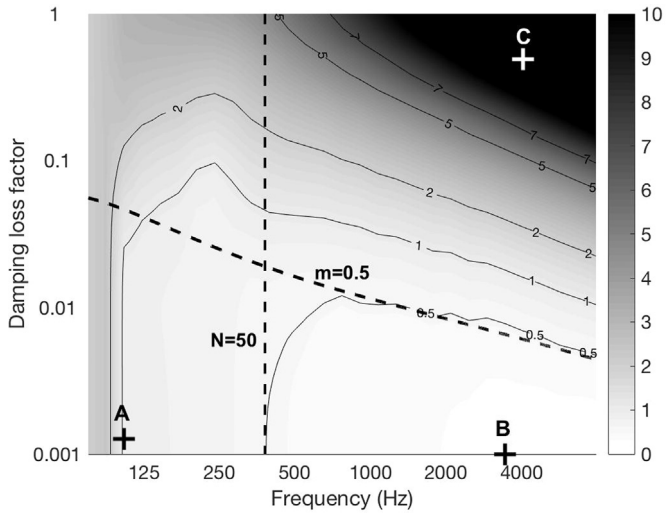

Fig. 7. Relative standard deviation of spatial energy repartition in the frequency, damping loss factor plane under a point-excitation. Left side, zone of modal behaviour with few modes contributing the dynamics. Top right-hand corner (black), zone of free field where rays are highly absorbed. Bottom right-hand corner (bright), zone of diffuse field.

has been finely calculated by Eq. (16). The total number of modes is 14,950 including all modes $0 \le i \le 149$ and $1 \le j \le 50$. The highest natural frequency is 87 kHz. All modes have the same damping loss factor $\eta_\alpha = \eta$. The expectation of local energy is then calculated by Eq. (33) at 10,000 receiver points chosen at random on the plate. The frequency integration is performed over octave bands $\Delta\omega = \omega_0/\sqrt{2}$ centred on ω_0 with a frequency step of $\eta\omega_0/4$ to ensure a fine representation of the frequency evolution. These calculations have been performed for 30 octave bands from 63 Hz to 8 kHz (the octave bands overlap) and for 30 damping loss factors ranging from 0.001 to 1.

Fig. 7 shows the values of the relative spatial standard deviation σ in the ω_0, η-plane. We can observe several zones corresponding to different states of the vibrational field. At low frequencies, on the left side of the map, we find the modal field regime characterised by values of σ of order of unit (100% of spatial fluctuations). At high frequencies and high damping, in the top right-hand corner of the map, is the regime of free field where σ can reach very large values (up to 700%). And at high frequencies and low damping, in the bottom right-hand corner of the map, we find the regime of diffuse field. This is the regime where σ is small indicating a uniform repartition of vibrational energy. These observations are similar to those made on isotropic plates in Ref. [34].

In the regime of modal field, the dynamics is dominated by one or few modes. Since the modes of a plate are global, the vibration extends to the entire tyre with an alternation of modal lines and antinodes. An example of modal field is shown in Fig. 8(a). The frequency bandwidth is the octave centred on 104 Hz and the damping loss factor is $\eta = 0.0013$ which corresponds to point A in Fig. 7. The band contains only three natural frequencies (five modes) whose subscripts (i,j) are (0, 1), (1, 1), and (2, 1). They have respectively 0, 1, and 2 wavelengths in the circumference length and one half-wavelength in the width. The first mode is difficult to observe in Fig. 8(a). But the other two modes with respectively two and four maxima of energy in the circumferential direction are clearly recognisable from Fig. 8(a).

The regime of diffuse field is characterised by low values of σ (bottom right-hand corner of Fig. 7). In this regime, the energy is more or less uniformly distributed over the tyre surface as shown in Fig. 8(b) for point B in Fig. 7. Two parameters are sufficient to delimit the zone of diffuse field. The diffuse state is reached only if the mode count is sufficiently high to ensure that no particular mode dominates the dynamics. In Fig. 7, the black broken vertical line indicates the limit $N=50$ modes per octave band. The zone of diffuse field that we may define for instance by a relative standard deviation of energy less than 50% ($\sigma < 0.5$) is well delimited by this line on its left side (lowest frequency). As we have noted in Section 3.4 the second condition for diffuseness is a low attenuation. The line of isovalues $m=0.5$ is plotted in Fig. 7 by a second broken line. We may observe that this line well gives the upper limit of the diffuse field zone $\sigma < 0.5$. Note that an accurate calculation of σ at high frequencies requires a very high number of receivers (10,000 in the present simulation).

The regime of free field (or direct field) is characterised by high values of σ (top right-hand corner of Fig. 7). These high values are explained by a confinement of the energy in the vicinity of the driving point. The field being dominated by the direct field, the energy density around the source is $P\exp(-\eta\omega r/c_g)/2\pi c_g r$ where r is the source receiver distance and P the source power in W. Since the mean energy in the plate is $P/\eta\omega$, we may introduce by analogy with room acoustics the critical distance D_c by the equality

$$P\frac{\exp(-\eta\omega D_c/c_g)}{2\pi c_g D_c} = \frac{P}{\eta\omega} \tag{36}$$

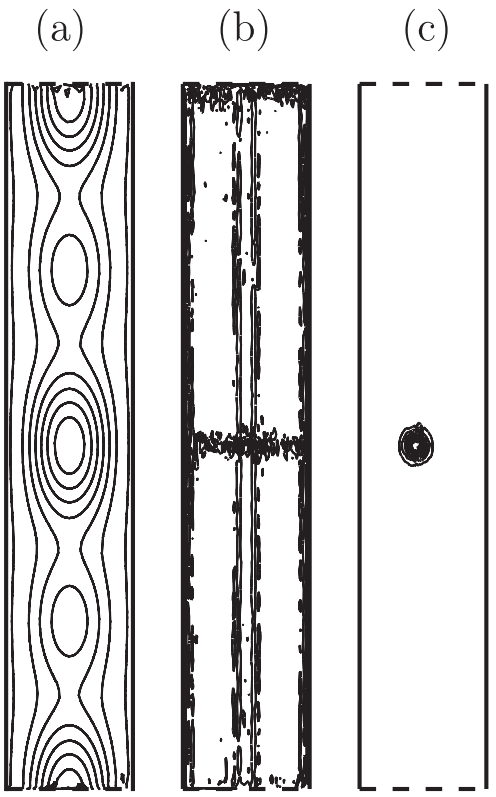

Fig. 8. Examples of energy fields corresponding to crosses in Fig. 7. (a), Regime of modal field (point *A*). (b), Regime of diffuse field (point *B*). (c), Regime of free field (point *C*).

When the damping term $\exp(-\eta\omega r/c_g)$ does not dominate the geometrical decreasing $1/r$, the critical distance is

$$D_c = \frac{\eta\omega}{2\pi c_g} \tag{37}$$

The critical distance gives the extent of the direct field. Beyond this limit, the vibrational field is reverberant. For instance, in Fig. 8(c) is shown an example of vibrational response of the tyre for the octave band centred on 4 kHz with a high damping $\eta = 50\%$ which corresponds to point *C* in Fig. 7. The critical distance is $D_c = 9$ m where the group speed $c_g = 225$ m/s is taken from Fig. 3(b). This critical distance being larger than the size of the tyre, this means that the vibrational field is entirely dominated by the direct field.

5. Effect of contact zone

Actual tyres are not excited by one but by several contact points in the contact zone. In the case of multipoint excitation, Eq. (33) must be modified. If the forces are mutually uncorrelated, then the power spectral density of vibrational speed is given by a linear superposition $S_{\dot{v}\dot{v}}(\omega) = \sum_j \left|Y(\mathbf{x}, \mathbf{x}_j; \omega)\right|^2 S_j$ where $\mathbf{x}_j$, $j = 1, 2, \ldots$ are the positions of the point forces and S_j their power spectral densities. But the point sources have the same power spectral density S_0 (rain-on-the-roof excitation) then the local energy becomes

$$E(\mathbf{x};\, \omega_0) = S_0 \sum_j \int_{\Delta\omega} m \left|Y(\mathbf{x}, \mathbf{x}_j;\, \omega)\right|^2 \mathrm{d}\omega \tag{38}$$

where again, the integration is performed over the octave band $\Delta\omega$ of interest. All the rest of the calculations is similar to the single point case. In particular, the transfer mobility $Y(\mathbf{x}, \mathbf{x}_j, ;\, \omega)$ between the source $\mathbf{x}_j$ and the receiver $\mathbf{x}$ is always given by Eq. (16).

The numerical simulation is performed with the same numerical values as in Section 4.3 except that now, the number of point forces is $N_s = 10$. The positions of these point forces has been chosen at random in the contact zone defined by a square of 10 cm length centred on the tyre $(a/2, b/2)$.

Fig. 9 shows the map of relative standard deviation σ in ω, η-plane for a multipoint excitation. The same three regimes, modal, diffuse field and free field are of course present. But compared with Fig. 7, we may observe that the diffuse field zone

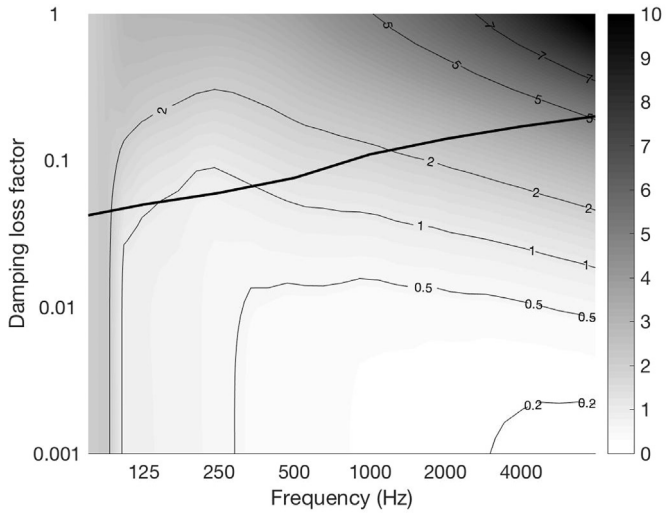

Fig. 9. Relative standard deviation of spatial energy repartition in the frequency, damping loss factor plane under a contact zone. Black solid line, realistic frequency-damping law.

is enlarged. The repartition of excitation over the surface of the tyre tends to homogenize the energy. In the limit case of a uniform excitation over the full surface would lead to a diffuse field whatever the level of damping. The solid black line in Fig. 9 indicates the actual position of a tyre for a typical evolution of the damping loss factor. It is apparent that the zone of diffuse field is never reached by actual tyres. The transition from low to high frequencies is made without passing in the diffuse field zone. Actual tyres therefore experiment only two regimes, the modal regime at low frequencies and the free field regime at higher frequencies. Above the transition frequency (400 Hz in the present simulation), the vibrational energy remains confined in the vicinity of the contact zone. This conclusion is well confirmed by experimental observations [35].

6. Conclusion

In conclusion, the model of prestressed orthotropic plate on visco-elastic foundation shows that the vibrational behaviour of a tyre may be separated in two distinct frequency bands.

At low frequencies, the elastic foundation imposes a cut-on frequency for wave propagation. Above cut-on, a single wave propagates with a speed dependent on the direction. The dispersion relationship (23) shows that all effects are important in the resulting dynamics including the elastic foundation, tension of membrane imposed by inflating pressure and bending rigidity due the structural composition of tyres. At low frequencies, the point mobility presents well separated peaks at the first natural frequencies of tyre. In this modal regime, the dynamics is dominated by few modes (typically of order of six) whose modal overlap is relatively low (less than 0.2).

At high frequencies, beyond 400 Hz in the present simulation, the mode count and the modal overlap increase drastically. The dynamics is mainly driven by bending effects. The behaviour of individual modes is longer observable on point mobility. In this non modal domain, the geometrical acoustics approach is valid and the energy field may be described in terms of rays. Rays propagate in straight lines but with a speed depending on the direction.

The transition from low to high frequencies has been investigated in the frequency, damping loss factor plane. In general, three regimes exist in plates which are the modal, diffuse field, and free field regimes. For realistic tyres, damping is relatively high and increases with frequency. The actual trajectory in the diffuse field map of Fig. 9 shows that at low frequency, the field is modal while at high frequencies, above 400 Hz, the attenuation per mean-free-path is high and the free field dominates. The transition from the modal regime to the free field regime is direct and the diffuse field state is generally not reached by actual tyres.

Acknowledgement

This work was supported by the Labex CeLyA of Université de Lyon, operated by the French National Research Agency (ANR-10-LABX-0060/ANR-11-IDEX-0007). This support is greatly appreciated.

References

[1] ENNAH - European Network on Noise and Health, final report, 2008, Available at: ⟨https://ec.europa.eu/jrc/en/publication/eur-scientific-and-technical-research-reports/final-report-ennah-european-network-noise-and-health-project⟩.
[2] U. Sandberg, Tyre/road noise - Myths and realities, Proceeding of the International Congress and Exhibition on Noise Control Engineering, INTER-NOISE 2001, The Hague, The Netherlands, 27–30 August, 2001.
[3] M.-A. Pallas, J. Kennedy, I. Walker, M. Bérengier, J. Lelong, FOREVER - Noise emission of electric and hybrid electric vehicles, *Report FOREVER-WP2* D2 (2013).
[4] U. Sandberg, G. Descornet, Road surface influence on tyre/road noise - Part I, G. Descornet, U. Sandberg, Road surface influence on tyre/road noise - Part II, Proceeding of the International Conference on Noise Control Engineering, INTER-NOISE 80, Miami, Florida, 8–10 December, 1980.
[5] M. Brinkmeier, U. Nackenhorst, S. Petersen, O. von Estorff, A finite element approach for the simulation of tire rolling noise, *J. Sound Vib.* 309 (2008) 20–39.
[6] E. Rustighi, S.J. Elliott, S. Finnveden, K. Gulyás, T. Mócsai, M. Danti, Linear stochastic evaluation of tyre vibration due to tyre/road excitation, *J. Sound Vib.* 310 (2008) 1112–1127.
[7] D.J. O'Boy, A.P. Dowling, Tyre/road interaction noise - numerical noise prediction of a patterned tyre on a rough road surface, *J. Sound Vib.* 323 (2009) 270–291.
[8] W. Kropp, P. Sabiniarz, H. Brick, T. Beckenbauer, On the sound radiation of a rolling tyre, *J. Sound Vib.* 331 (2012) 1789–1805.
[9] W. Kropp, Ein Modell zur Beschreibung des Rollgeräusches eines unprofilierten Gürtelreifens auf rauher Straenoberfläche [A model for the description of the rolling noise of a smooth tyre on a rough road surface]. Doctoral thesis in Fortschritt-Berichte Reihe 11, Nr 166, VDI Verlag, Düsseldorf, 1992.
[10] Y.B. Chang, T.Y. Yang, W. Soedel, Dynamic analysis of a radial tire by finite elements and modal expansion, *J. Sound Vib.* 96 (1984) 1–11.
[11] S. Saigal, T.Y. Yang, H.W. Kim, W. Soedel, Free vibration of a tire as a toroidal membrane, *J. Sound Vib.* 107 (1986) 71–82.
[12] T.L. Richards, Finite element analysis of structural-acoustic coupling in tyres, *J. Sound Vib.* 149 (1991) 235–243.
[13] Y. Nakashima, J.Y. Wong, A three dimensional tire model by the finite element method, *J. Terramechanic* 30 (1993) 21–34.
[14] C.M. Nilsson, Waveguide finite elements applied on a car tyre, doctoral thesis, Royal Institute of Technology, 2004.
[15] D. Duhamel, B.R. Mace, M.J. Brennan, Finite element analysis of the vibrations of waveguides and periodic structures, *J. Sound Vib.* 294 (2006) 205–220.
[16] S. Finnveden, M. Fraggstedt, Waveguide finite elements for curved structures, *J. Sound Vib.* 312 (2008) 644–671.
[17] Y. Waki, B.R. Mace, M.J. Brennan, Free and forced vibrations of a tire using wave/finite element approach, *J. Sound Vib.* 323 (2009) 737–756.
[18] Dodge R.N., S.K. Clark & B. Vahidi, The dynamic stiffness of a pneumatique tire model. Society of automotive engineers. Department of Engineering Mechanics, University of Michigan, March 1965.
[19] W. Kropp, Structure-borne in a smooth tyre, *Appl. Acoust.* 26 (1989) 181–192.
[20] C.R. Dorhman, Dynamics of tyre wheel suspension assembly, *J. Sound Vib.* 210 (1998) 627–642.
[21] W. Soedel, M.G. Prasad, Calculation of natural frequencies and modes of tires in road contact by utilizing eigenvalues of the axisymmetric non-contacting tire, *J. Sound Vib.* 70 (1980) 573–584.
[22] K. Larsson, W. Kropp, A high-frequency three-dimensional tyre model based on two coupled elastic layers, *J. Sound Vib.* 253 (2002) 889–908.
[23] J.F. Hamet, Tire/road noise: *time domain green's function for the orthotropic plate model*, *Acta Acoustica* 87 (2001) 470–474.
[24] P.B.U. Andersson, W. Kropp, Time domain contact model for tyre/road interaction including nonlinear contact stiffness due to small-scale roughness, *J. Sound Vib.* 318 (2008) 296–312.
[25] G. Dubois, J. Cesbron, H.P. Yin, F. Anfosso-Lédée, Numerical evaluation of tyre/road contact pressures using a multi-asperity approach, *Int. J. Mech. Sci.* 54 (2012) 84–94.
[26] J. Cesbron, F. Anfosso-Lédée, D. Duhamel, H.P. Yin, D. Le Houédec, Experimental study of tyre/road contact forces in rolling conditions for noise prediction, *J. Sound Vib.* 320 (2009) 125–144.
[27] J. Périsse, J.M. Clairet, J.F. Hamet, Modal testing of a smooth tire in low and medium frequency-estimation of structural parameters, in: Proceedings of 18th International Modal Analysis Conference, San Antonio, USA, 7–10 February, 2000, pp. 960–967.
[28] P. Andersson, K. Larsson, W. Kropp, A method for experimental collection of global material data for tires, *Nordic Vib. Res.* (2001).
[29] R. Langley, The modal density of anisotropic structural components, *J. Acoust. Soc. Am.* 99 (1996) 3481–3487.
[30] A. Bourgine, Sur une approche statistique de la dynamique vibratoire des structures [On a statistical approach of structural vibrations]. Doctoral thesis in Université Paris-Sud, Nr 1134, Orsay, 1973.
[31] A. Le Bot, V. Cotoni, Validity diagrams of statistical energy analysis, *J. Sound Vib.* 329 (2010) 221–235.
[32] A. Le Bot, *Foundation of statistical energy analysis in vibroacoustics*, Oxford University Press, Oxford, 2015.
[33] J. Davy, R. Weaver, Comment on Relative variance of the mean squared pressure in multimode media: *rehabilitating former approaches*, *J. Acoust. Soc. Am.* 136 (2014) 2621–2629.
[34] T. Lafont, N. Totaro, A. Le Bot, Review of statistical energy analysis hypotheses in vibroacoustics, Proc. R. Soc. A 470 (2013) 20130515.
[35] J. Perisse, A study of radial vibrations of a rolling tyre for tyre-road noise characterisation, *Mech. Syst. Signal Process.* 16 (2002) 1043–1058.